Tracking the Ionization Site in Neutral Molecules

L. Ortmann,[1,2,*] A. AlShafey,[2] A. Staudte,[3] and A. S. Landsman[2,†]
[1]Max Planck Institute for the Physics of Complex Systems, Nöthnitzer Straße 38, D-01187 Dresden, Germany
[2]Department of Physics, The Ohio State University, Columbus, Ohio 43210, USA
[3]Joint Attosecond Science Lab of the National Research Council and the University of Ottawa, Ottawa, Ontario K1A 0R6, Canada

(Received 16 October 2020; revised 19 September 2021; accepted 15 October 2021; published 16 November 2021)

When a diatomic molecule is exposed to intense light, the valence electron may tunnel from a higher potential (corresponding to an upfield atom) due to the suppressed internuclear barrier. This process is known as ionization enhancement and is a key mechanism in strong field ionization of molecules. Alternatively, the bound electron wave function can evolve adiabatically in the laser field, resulting in ionization from the downfield atom. Here, we introduce a method to quantify the relative contribution of these two processes. Applying this method to experimentally measured electron momenta distributions following strong field ionization of N_2 with infrared laser light, we find approximately a 2:1 ratio of electrons ionized from a downfield atom, relative to upfield. This suggests that the bound state wave function largely adapts adiabatically to the changing laser field, although the nonadiabatic process of ionization enhancement still contributes even in neutral molecules. Our method can be applied to any diatomic neutral molecule to better understand the evolution of the initially bound electron wave packet and hence the nature of the molecular ionization process.

DOI: 10.1103/PhysRevLett.127.213201

Tunnel ionization is a key process in attosecond science. It constitutes the first step in high-harmonic generation [1,2], attoclock experiments [3,4], and self-interrogating imaging techniques, such as photoelectron holography [5–11] or molecular orbital tomography [12–16]. The interpretation of all of these processes strongly depends on the localization of the electron wave packet immediately after tunneling.

The location of the electron subsequent to tunnel ionization is already important in isolated atoms [17–19], but becomes even more crucial in molecules, where the electron can tunnel from any of its constituent atoms. To complicate matters, the Coulomb potential of one atom is not only distorted by the laser field but by the Coulomb potential of the other atom [20,21]. This additional distortion can lower the tunneling barrier for electrons located at the upfield nucleus (see Fig. 1), leading to enhanced ionization [20–39].

Enhanced ionization has been extensively studied over the last decades [20–39]. The underlying mechanism relies on the electron tunneling from the upfield atomic site when the direction of the laser field points along the internuclear axis, as can be seen from Fig. 1. Alternatively, the laser field can shift the bound electron wave packet toward the downfield atom and the electron may start tunneling out of the molecule from there. This adiabatic adaption of the electron position to the laser field is commonly expected to occur if the internuclear distance is small and the laser field changes relatively slowly. Consequently, for enhanced ionization, the potential barrier has to move sufficiently fast to allow trapping of the electron in the upper well [20,21,26,33–35,40]. Here, we show how to *quantitatively* distinguish between these two basic mechanisms, thereby

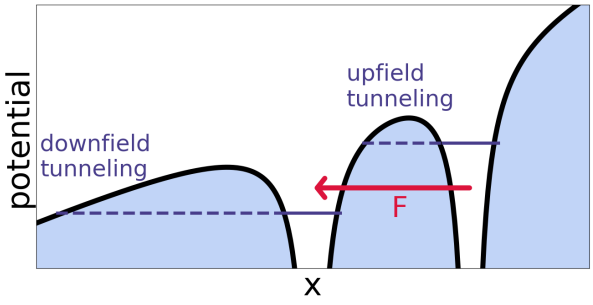

FIG. 1. Illustration of a diatomic potential for alignment of the internuclear axis along the polarization axis. The ionization barrier for the upper well is considerably lowered by the influence of the lower well, which can lead to ionization enhancement. However, the force F of the electric field can drive the electron toward the downfield well, which is expected to play a role if the electron position adapts adiabatically to the laser field.

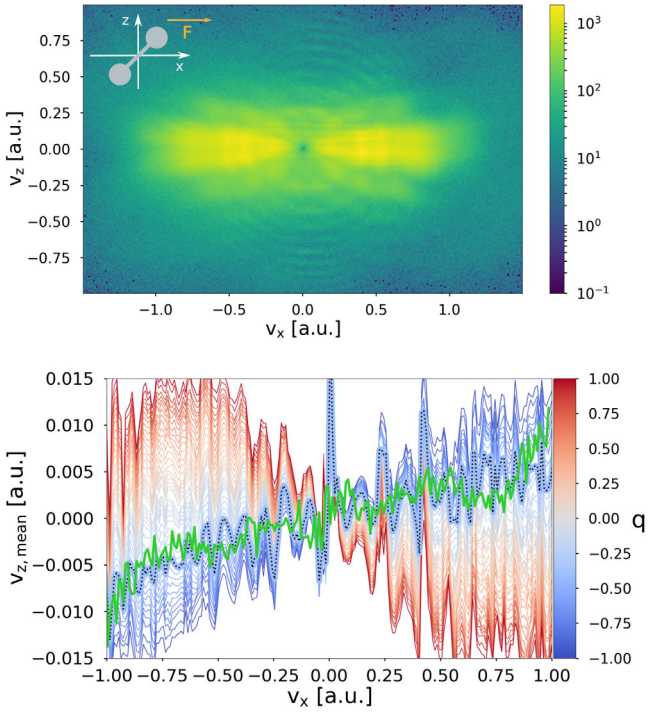

FIG. 2. Top panel: experimental 2D photoelectron momentum distribution for the 45° case from [43]. The inset shows a sketch of the molecular orientation and the laser polarization direction. Bottom panel: $v_{z,\mathrm{mean}}$ as a function of v_x. The green line represents the values extracted from the experimental data (top panel) minus the orientation averaged experimental data (for details see Supplemental Material [44]). The ensemble of curves was obtained from QTMC simulations over a range of ionization ratios q, which is specified by the color of the curve (see color bar). The theoretical curve that matches the experimental data best according to the average offset momentum a (see Fig. 4) is shown as a bold line with black dashes. In both the theoretical and experimental evaluation leading to the displayed curves the 2D momentum distribution was restricted to $v_x \in [-1, 1]$ and $v_z \in [-1, 1]$.

illuminating key details of the strong field molecular ionization process.

Prior studies have focused on dissociative ionization channels where multiple electrons are released, leading to Coulomb explosion [22–24,26–28,30–32,37,38,41]. In this case, enhanced ionization is believed to play a dominant role due to the bond stretching of the dissociating molecular ion [21]. Coulomb explosion, however, does not allow for determination of the ionization site in the neutral homonuclear molecule. Recently, another method was proposed in [39] for the determination of the tunneling site which does not use Coulomb explosion and could therefore be applied to neutral molecules. However, this method does not quantify the likelihood of electrons being ionized from the two different atomic sites, and hence is not able to predict the relative contributions from adiabatic versus enhanced molecular ionization channels. Moreover, for reconstruction methods such as photoelectron holography [5–11] or molecular orbital tomography [12–16], a quantitative answer to the ionization site question is obviously vital.

Here, we introduce a method for quantitatively retrieving the ratio of ionization events at the upfield and downfield atomic site in a diatomic molecule by comparing experimental data with quantum trajectory Monte Carlo simulations (QTMC). Note that the atoms A and B in a diatomic molecule AB change from being the upfield or downfield atom several times during the laser pulse, as the sign of the electric field changes. Here, we study the relative contribution of ionization from the upfield and downfield atom rather than from atom A or B.

Our technique is based on the electron's deflection in the asymmetric Coulomb potential of the molecule that is tilted against the laser polarization direction. This introduces an asymmetry in the final photoelectron momentum distribution, which depends on the ratio of electrons born at the upfield or downfield atom. We apply this method to experimental data from strong field ionization of a neutral N_2 molecule with infrared laser light. We find that although adiabatic evolution of the bound electron wave function (leading to increased downfield ionization) dominates for neutral molecules, nonadiabatic enhanced ionization still makes a significant contribution under typical experimental conditions, corresponding to the intermediate value of the Keldysh parameter, $\gamma \approx 1$ [42], where $\gamma = \omega\sqrt{2I_p}/F$, with ω, F, and I_p the laser frequency, peak field, and ionization potential of the molecule, respectively.

Figure 2 (top panel) shows an experimentally measured 2D photoelectron momentum distribution from an N_2 molecule tilted 45° against the laser polarization in the x direction. The details on the experimental procedure can be found in [43]. The average of the transverse momenta v_z for each momentum v_x along the polarization direction is calculated using

$$v_{z,\mathrm{mean}}[v_x(i)] = \frac{\sum_{j=1}^{n} w(i,j) v_z(j)}{\sum_{j=1}^{n} w(i,j)}, \tag{1}$$

where $w(i, j)$ is the two-dimensional momentum distribution of the detected photoelectron momenta with the ith and jth bins of the histogram along v_x and v_z, respectively. This quantity, as extracted from the experimental data, is plotted as a bold green line in the bottom panel of Fig. 2 and clearly shows asymmetry. For parallel and perpendicularly aligned molecules, the 2D momentum distribution is mirror symmetric with respect to the $v_z = 0$ line and $v_{z,\mathrm{mean}}(v_x)$ would be a horizontal line.

In order to understand the momentum offset, we perform QTMC simulations [45], where we include the corrections proposed in [46] and the phase due to the spatial offset of the ionized electron introduced in [47]. Detail on how to estimate Coulomb corrections in the atomic case, and more

general formal insight into the justification underlying the two-step propagation process can be found in [48,49]. A comparison between the experimental data of strong field ionization of the OCS molecule, a two-step classical propagation model, and time-dependent density-functional theory can be found in [50].

We use a neutral N_2 molecule tilted against the laser polarization direction by 45°. The tilt of the molecule results in an asymmetry, an offset momentum $v_{z,\mathrm{mean}}(v_x) \neq 0$, of the electron momentum distribution at the detector. As we will show, the degree of asymmetry depends on the relative probability of the electron being born at the upfield or downfield atomic site.

In the simulation, the peak laser intensity is given by $I = 1.3 \times 10^{14}$ W/cm^2 and the wavelength set to 800 nm, as in the experiment [43,51]. The laser, polarized along the x axis, is six cycles long under a $\cos^2$ envelope, with ionization potential set to $I_p = 15.6$ eV [43]. The experimental intensity variation in the focal volume is theoretically accounted for by focal averaging [47,52,53].

The shape of the molecular orbital contributing an electron is calculated with GAMESS [54], and used to obtain the initial transverse momentum distribution via the partial Fourier transform approach [55,56]. Nonadiabatic initial conditions are used at the tunnel exit [57] (see Supplemental Material [44] for detail). The Coulomb potential is included in the propagation, following the method in [43,47], and using an equilibrium molecular bond distance of 2 a.u., obtained from the literature [58,59].

To determine the relative probabilities of ionization from the upfield and downfield potential wells, we vary the fraction of electrons born at the upfield and downfield site in theory and find the value that gives the best agreement with the experimental result. To this end, we define the ratio of ionization sites q as

$$q = \frac{\mathrm{no.up} - \mathrm{no.down}}{\mathrm{no.up} + \mathrm{no.down}}, \tag{2}$$

where no.up and no.down are the number of electrons born upfield and downfield, respectively. The limits of $q = -1$ and $q = +1$ therefore correspond to the electrons being born exclusively at the downfield or upfield atom, respectively. For our calculations, we select 42 different ratios q, thus obtaining a discrete mapping of q to the observable asymmetry in the momentum distribution, i.e., the average offset momentum a. This result can be used to extract the upfield-to-downfield ratio from the experimental data.

The bottom panel of Fig. 2 shows the QTMC results, $v_{z,\mathrm{mean}}(v_x)$, over a range of ionization ratios q, specified in the color bar. The evaluation of the final momentum distribution was done the same way as in the experiment, which limits integration over v_y to an out-of-plane angle of $\theta < 10°$ before calculating $v_{z,\mathrm{mean}}(v_x)$. The theoretical $v_{z,\mathrm{mean}}(v_x)$ curves exhibit a clear pattern: the more electrons are ionized from the upfield atom (redder on the color bar), the more positive is $v_{z,\mathrm{mean}}$ for $v_x < 0$ and the more negative for $v_x > 0$. If the majority of electrons is born at the downfield atom, the signs are reversed.

We explain the origin of the asymmetry in $v_{z,\mathrm{mean}}(v_x)$ shown in Fig. 2, by analyzing QTMC trajectories. Quantum trajectory analysis shows that the asymmetry is caused by the asymmetric Coulomb potential of the molecule, with illustration of the underlying mechanism shown in Fig. 3. Without loss of generality, we focus on those electrons that are born when the vector potential A was negative and that end up at $v_x > 0$. As the depiction of the pulse in the top panel of Fig. 3 shows, $A < 0$ can either happen at a positive field strength that is decreasing (green) or at a negative field strength whose absolute value is increasing (orange). The four lower panels each show two trajectories with initial transverse velocities of opposite sign but identical absolute value. In each case, the degree of deflection of those two trajectories differs due to the asymmetry of the Coulomb potential. We quantify the difference of the deflections of the two trajectories by defining the overall deflection Δv_z as the sum of changes in v_z of the two trajectories from the birth in the continuum till after the pulse has passed

$$\Delta v_z = (v^+_{z,f} - v^+_{z,i}) + (v^-_{z,f} - v^-_{z,i}) = v^+_{z,f} + v^-_{z,f}, \tag{3}$$

where i and f denote the initial and final condition of the trajectory and the superscripts $+$ and $-$ mark the opposite signs in the initial velocity of the two trajectories.

In the left half of the lower panels in Fig. 3 (green, corresponding to a positive field strength that is decreasing) the overall deflection Δv_z of an electron born at the upfield atom is negative due to the pull from the downfield atom. Vice versa, if the electron is born at the downfield atom, Δv_z is positive. That is also the effect we observed in the bottom panel of Fig. 2, where $v_{z,\mathrm{mean}}$ is positive for electrons mostly born at the downfield site (blue curves) and negative for electrons mostly born at the upfield site (red curves) in the regime $v_x > 0$.

Following a reversal of the laser field, a previously downfield atom becomes upfield, and vice versa. Consequently, also the signs of the overall deflections are inverted: positive for a birth at the upfield atom and negative for a birth at the downfield atom. For all cases, as Fig. 3 suggests (see trajectory analysis in the Supplemental Material [44] for more detail), the asymmetric deflection is smaller for the electrons which directly leave the parent ion (orange), compared to the case when the electron goes around the parent ion on its way to the detector (green).

To sum up, even though the overall deflections Δv_z have opposite signs in adjacent quarter cycles (with the same sign of A), they do not compensate each other. This is because the deflection in the "green" quarter cycles dominates, since in these cases the electron revisits the vicinity of the parent ion and is therefore deflected by the

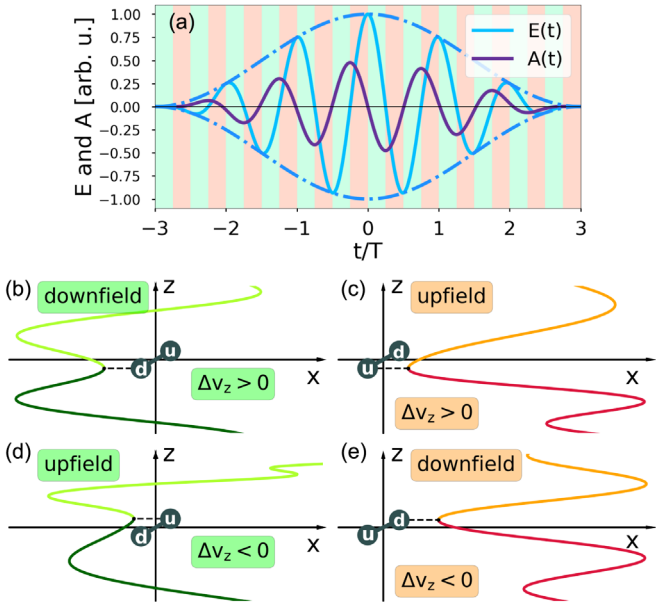

FIG. 3. (a) Field strength and vector potential in the pulse. Quarter cycles with decreasing absolute field strength are highlighted in green, whereas increasing absolute field strengths are marked in orange. (b),(d) Decreasing absolute field strength. Each panel shows two trajectories of electrons with an initial transverse momentum of the same absolute value but opposite sign. The two electrons go around the parent molecular ion and the fact that they are deflected differently results in an asymmetry of the momentum distribution at the detector. (c),(e) Increasing absolute field strength. The electrons have a positive final velocity again because the same sign of A is chosen. The electrons go directly to the detector and are deflected less strongly by the asymmetric Coulomb potential. Note that these trajectories were calculated with an oversized molecule for illustrative purposes. For an accurate calculation with trajectories of the real system we refer to Supplemental Material [44].

asymmetric Coulomb potential more strongly. An analogous line of reasoning can be applied to $v_x < 0$, where the signs of the deflections need to be swapped. This explains qualitatively the nonzero offset momentum $v_{z,\mathrm{mean}}$ observed in the bottom panel of Fig. 2.

To describe the asymmetry observed in the experiment and in the QTMC simulations quantitatively, we define the average offset momentum a as follows:

$$a = \frac{\sum_{i=1}^{m} \mathrm{sign}[v_x(i)] v_{z,\mathrm{mean}}[v_x(i)]}{m}. \tag{4}$$

The meaning of this definition becomes clear when looking again at the bottom panel of Fig. 2, where a large deviation of the offset momentum $v_{z,\mathrm{mean}}$ from zero corresponds to a more asymmetric 2D momentum distribution. In the above formula, $\sum v_{z,\mathrm{mean}}/m$ calculates the average deviation from the horizontal line and multiplication by the sign of v_x at every bin, first, prevents the opposite signs of the offset momentum $v_{z,\mathrm{mean}}$ (for $v_x < 0$ and $v_x > 0$) from canceling in the summation and, second, enables us to distinguish between the $v_{z,\mathrm{mean}}$ curves rising or falling, thus leading to a unique mapping between q and a.

We now compare the experimental average offset momentum against a range of ionization ratios in the QTMC simulations. The result is depicted in Fig. 4. Comparing the experimental value of $a = 3.17 \times 10^{-3} \pm 6.4 \times 10^{-5}$ a.u. with the theoretical curve now allows us to estimate the ionization ratio of the upfield and downfield atoms in the experiment (see Supplemental Material [44] for details of the error bar). The value obtained is $q = -0.379 \pm 6 \times 10^{-3}$, which means for every electron born upfield, roughly two electrons are born downfield. The roughly 2:1 predominance of downfield over upfield ionization suggests that for neutral molecules, ionization due to the adiabatic evolution of the wave function in the laser field somewhat dominates over enhanced ionization.

To conclude, we found that the degree of asymmetry in deflection of electrons released from a molecule tilted against the laser polarization can be used to estimate the ratio of electrons born at the upfield and downfield atom. Applying this method to experimental data for the ionization of N_2, we find that ionization primarily happens at the downfield atom. As the tunneling barrier would be narrower at the upfield atom, this indicates that the bound electron wave function adapts adiabatically to the laser field. More generally, this method therefore allows insights into the time-dependent electron response inside the molecule.

In contrast to prior work that focused on ionization of charged molecules that defragment after ionization, our approach is also applicable to neutral molecules. It is also not necessary to have different atomic species involved, as opposed to Ref. [32], which made a crucial contribution to the question of the ionization site in $ArXe^+$. The technique presented here, in contrast, can be applied to homonuclear molecules.

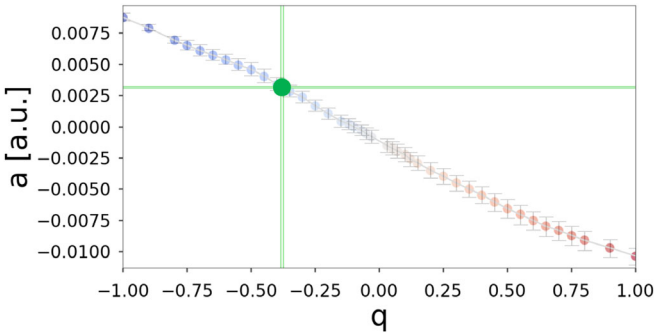

FIG. 4. Average offset momentum a according to Eq. (4) as a function of the ionization site ratio q according to Eq. (2). The colors of the dots are chosen according to the color coding for q in the color bar of Fig. 2. The error bars denote the uncertainty for $\pm 5°$ deviations from 45° orientation. The experimental value is plotted as a larger green dot, with the horizontal and vertical green lines at the upper and lower error bar.

Finally, note that our method allows for a quantitative answer to the question of the ionization site, thus going beyond the merely qualitative treatment in [39]. This is especially relevant whenever accurate theoretical models are required to reconstruct information from experimental measurements that involve ionization and recollision or recombination, such as the case in many imaging techniques. Moreover, the model proposed here can also be applied to heteronuclear molecules and holography data that do not actively align the molecule, i.e., postaligned molecules [7].

The recent emphasis on including the Coulomb potential in reconstruction theories for photoelectron holography [8,60–65] or molecular orbital tomography [13,15,66] makes clear the need for quantitative information about the tunneling site, since it determines the electron's path and hence the parts of the Coulomb potential it is exposed to. The proposed method can therefore provide information required to attain higher accuracy in ultrafast imaging techniques.

This work was supported by the U.S. Department of Energy, Office of Basic Energy Sciences, Atomic, Molecular and Optical Sciences Program under Award No. DE-SC0022093.

*ortmann.1@osu.edu
†landsman.7@osu.edu

[1] A. L'Huillier and P. Balcou, Phys. Rev. Lett. **70**, 774 (1993).
[2] P. B. Corkum, Phys. Rev. Lett. **71**, 1994 (1993).
[3] A. S. Landsman and U. Keller, Phys. Rep. **547**, 1 (2015).
[4] C. Hofmann, A. S. Landsman, and U. Keller, J. Mod. Opt. **66**, 1052 (2019).
[5] Y. Huismans, A. Rouzée, A. Gijsbertsen, J. Jungmann, A. Smolkowska, P. Logman, F. Lepine, C. Cauchy, S. Zamith, T. Marchenko *et al.*, Science **331**, 61 (2011).
[6] X.-B. Bian and A. D. Bandrauk, Phys. Rev. Lett. **108**, 263003 (2012).
[7] M. Haertelt, X.-B. Bian, M. Spanner, A. Staudte, and P. B. Corkum, Phys. Rev. Lett. **116**, 133001 (2016).
[8] X. Song, C. Lin, Z. Sheng, P. Liu, Z. Chen, W. Yang, S. Hu, C. D. Lin, and J. Chen, Sci. Rep. **6**, 28392 (2016).
[9] Y. Zhou, O. I. Tolstikhin, and T. Morishita, Phys. Rev. Lett. **116**, 173001 (2016).
[10] G. Porat, G. Alon, S. Rozen, O. Pedatzur, M. Krüger, D. Azoury, A. Natan, G. Orenstein, B. Bruner, M. Vrakking *et al.*, Nat. Commun. **9**, 2805 (2018).
[11] M. He, Y. Li, Y. Zhou, M. Li, W. Cao, and P. Lu, Phys. Rev. Lett. **120**, 133204 (2018).
[12] J. Itatani, J. Levesque, D. Zeidler, H. Niikura, H. Pépin, J.-C. Kieffer, P. B. Corkum, and D. M. Villeneuve, Nature (London) **432**, 867 (2004).
[13] C. Vozzi, M. Negro, F. Calegari, G. Sansone, M. Nisoli, S. De Silvestri, and S. Stagira, Nat. Phys. **7**, 822 (2011).
[14] C. Zhai, X. Zhu, P. Lan, F. Wang, L. He, W. Shi, Y. Li, M. Li, Q. Zhang, and P. Lu, Phys. Rev. A **95**, 033420 (2017).
[15] C. Zhai, L. He, P. Lan, X. Zhu, Y. Li, F. Wang, W. Shi, Q. Zhang, and P. Lu, Sci. Rep. **6**, 23236 (2016).
[16] Y. J. Chen, L. B. Fu, and J. Liu, Phys. Rev. Lett. **111**, 073902 (2013).
[17] A. N. Pfeiffer, C. Cirelli, M. Smolarski, D. Dimitrovski, M. Abu-Samha, L. B. Madsen, and U. Keller, Nat. Phys. **8**, 76 (2012).
[18] I. Ivanov, C. H. Nam, and K. T. Kim, Sci. Rep. **7**, 39919 (2017).
[19] R. Boge, C. Cirelli, A. S. Landsman, S. Heuser, A. Ludwig, J. Maurer, M. Weger, L. Gallmann, and U. Keller, Phys. Rev. Lett. **111**, 103003 (2013).
[20] T. Zuo and A. D. Bandrauk, Phys. Rev. A **52**, R2511 (1995).
[21] T. Seideman, M. Y. Ivanov, and P. B. Corkum, Phys. Rev. Lett. **75**, 2819 (1995).
[22] K. Codling, L. J. Frasinski, and P. A. Hatherly, J. Phys. B **22**, L321 (1989).
[23] K. Codling and L. Frasinski, J. Phys. B **26**, 783 (1993).
[24] S. Chelkowski and A. Bandrauk, J. Phys. B **28**, L723 (1995).
[25] E. Constant, H. Stapelfeldt, and P. B. Corkum, Phys. Rev. Lett. **76**, 4140 (1996).
[26] D. Normand and M. Schmidt, Phys. Rev. A **53**, R1958 (1996).
[27] A. Staudte, D. Pavičić, S. Chelkowski, D. Zeidler, M. Meckel, H. Niikura, M. Schöffler, S. Schössler, B. Ulrich, P. Rajeev *et al.*, Phys. Rev. Lett. **98**, 073003 (2007).
[28] K. J. Betsch, D. W. Pinkham, and R. R. Jones, Phys. Rev. Lett. **105**, 223002 (2010).
[29] L. Xin, H.-C. Qin, W.-Y. Wu, and F. He, Phys. Rev. A **92**, 063803 (2015).
[30] H. Xu, F. He, D. Kielpinski, R. Sang, and I. Litvinyuk, Sci. Rep. **5**, 13527 (2015).
[31] J. Wu, M. Meckel, S. Voss, H. Sann, M. Kunitski, L. P. H. Schmidt, A. Czasch, H. Kim, T. Jahnke, and R. Dörner, Phys. Rev. Lett. **108**, 043002 (2012).
[32] J. Wu, M. Meckel, L. P. H. Schmidt, M. Kunitski, S. Voss, H. Sann, H. Kim, T. Jahnke, A. Czasch, and R. Dörner, Nat. Commun. **3**, 1113 (2012).
[33] J. Posthumus, Rep. Prog. Phys. **67**, 623 (2004).
[34] A. Saenz, Phys. Rev. A **61**, 051402(R) (2000).
[35] M. Brewczyk and L. Frasinski, J. Phys. B **24**, L307 (1991).
[36] G. N. Gibson, R. R. Freeman, and T. J. McIlrath, Phys. Rev. Lett. **67**, 1230 (1991).
[37] T. Ergler, A. Rudenko, B. Feuerstein, K. Zrost, C. D. Schröter, R. Moshammer, and J. Ullrich, Phys. Rev. Lett. **95**, 093001 (2005).
[38] I. Bocharova, R. Karimi, E. F. Penka, J.-P. Brichta, P. Lassonde, X. Fu, J.-C. Kieffer, A. D. Bandrauk, I. Litvinyuk, J. Sanderson *et al.*, Phys. Rev. Lett. **107**, 063201 (2011).
[39] K. Liu and I. Barth, Phys. Rev. Lett. **119**, 243204 (2017).
[40] J. H. Posthumus, L. J. Frasinski, A. Giles, and K. Codling, J. Phys. B **28**, L349 (1995).
[41] G. N. Gibson, M. Li, C. Guo, and J. Neira, Phys. Rev. Lett. **79**, 2022 (1997).
[42] L. Keldysh *et al.*, Sov. Phys. JETP **20**, 1307 (1965).
[43] M. Meckel, A. Staudte, S. Patchkovskii, D. Villeneuve, P. Corkum, R. Dörner, and M. Spanner, Nat. Phys. **10**, 594 (2014).

[44] See Supplemental Material at http://link.aps.org/supplemental/10.1103/PhysRevLett.127.213201 for details on the methods applied in the main text.
[45] M. Li, J.-W. Geng, H. Liu, Y. Deng, C. Wu, L.-Y. Peng, Q. Gong, and Y. Liu, Phys. Rev. Lett. **112**, 113002 (2014).
[46] N. Shvetsov-Shilovski, M. Lein, L. Madsen, E. Räsänen, C. Lemell, J. Burgdörfer, D. Arbó, and K. Tőkési, Phys. Rev. A **94**, 013415 (2016).
[47] M.-M. Liu, M. Li, C. Wu, Q. Gong, A. Staudte, and Y. Liu, Phys. Rev. Lett. **116**, 163004 (2016).
[48] S. A. Kelvich, W. Becker, and S. P. Goreslavski, Phys. Rev. A **93**, 033411 (2016).
[49] W. Becker and M. Kleber, Phys. Scr. **94**, 023001 (2019).
[50] A. Trabattoni, J. Wiese, U. De Giovannini, J.-F. Olivieri, T. Mullins, J. Onvlee, S.-K. Son, B. Frusteri, A. Rubio, S. Trippel *et al.*, Nat. Commun. **11**, 2546 (2020).
[51] M. Meckel, Ph.D. thesis, Johann-Wolfgang-Goethe-Universität Frankfurt, 2011.
[52] S. Augst, D. D. Meyerhofer, D. Strickland, and S.-L. Chin, JOSA B **8**, 858 (1991).
[53] R. Kopold, W. Becker, M. Kleber, and G. Paulus, J. Phys. B **35**, 217 (2002).
[54] M. W. Schmidt, K. K. Baldridge, J. A. Boatz, S. T. Elbert, M. S. Gordon, J. H. Jensen, S. Koseki, N. Matsunaga, K. A. Nguyen, S. Su *et al.*, J. Comput. Chem. **14**, 1347 (1993).
[55] R. Murray, W.-K. Liu, and M. Y. Ivanov, Phys. Rev. A **81**, 023413 (2010).
[56] S. G. Walt, N. B. Ram, M. Atala, N. I. Shvetsov-Shilovski, A. Von Conta, D. Baykusheva, M. Lein, and H. J. Wörner, Nat. Commun. **8**, 15651 (2017).
[57] M. Li, J.-W. Geng, M. Han, M.-M. Liu, L.-Y. Peng, Q. Gong, and Y. Liu, Phys. Rev. A **93**, 013402 (2016).
[58] B.-P. Stoicheff, Can. J. Phys. **32**, 630 (1954).
[59] D. Page and J. Powles, Mol. Phys. **29**, 1287 (1975).
[60] H. Xie, M. Li, Y. Li, Y. Zhou, and P. Lu, Opt. Exp. **24**, 27726 (2016).
[61] G. Shi, J. Xu, H. Zhang, C. Lin, X. Song, J. Chen, and W. Yang, J. Phys. Conf. Ser. **869**, 012003 (2017).
[62] N. I. Shvetsov-Shilovski and M. Lein, Phys. Rev. A **97**, 013411 (2018).
[63] A. Maxwell and C. F. de Morisson Faria, J. Phys. B **51**, 124001 (2018).
[64] J. Daněk, Ph.D. thesis, Ruprecht-Karls-Universität Heidelberg, 2018.
[65] S. D. López and D. G. Arbó, Eur. Phys. J. D **73**, 28 (2019).
[66] Y. Li, X. Zhu, P. Lan, Q. Zhang, M. Qin, and P. Lu, Phys. Rev. A **89**, 045401 (2014).